Cyclic behavior of reinforced concrete L- and T-columns retrofitted from rectangular columns

Yu-Chen Ou[1,*] and An-Nhien Truong[2]

[1] Professor, Department of Civil Engineering,

National Taiwan University,

No. 1, Sec. 4, Roosevelt Rd., Taipei 10617, Taiwan

E-mail: yuchenou@ntu.edu.tw

Phone: +886-2-3366-4233

Fax: +886-2-2739-6752

* Corresponding author

[2] Former research assistant, Department of Civil and Construction Engineering,

National Taiwan University of Science and Technology

E-mail: pion.scor@gmail.com

Cyclic behavior of reinforced concrete L- and T-columns retrofitted from rectangular columns

ABSTRACT

An innovative seismic retrofit method was proposed to address the weak first-story issue of reinforced concrete row houses in Taiwan. The proposed method is to turn as-built rectangular columns to L- and T-columns by adding flanges in the weak direction of as-built rectangular columns to strengthen their seismic capacities. The longitudinal reinforcement in the retrofit part of the retrofitted column is not continuous into the beam and foundation above and below the column to ease construction difficulty associated with post-installation of such reinforcement. Large-scale L- and T-columns retrofitted from rectangular columns with the proposed retrofit method were tested in this research using lateral cyclic loading. Test results showed that the retrofitted columns exhibited ductile, flexural dominated behavior. As compared with the original rectangular columns, the proposed retrofit method was effective in increasing the lateral strength of the column. Due to the discontinuity of the longitudinal reinforcement, the retrofitted columns showed lower lateral strengths but less damage and higher ductility than the counterpart monolithic columns. A pushover analysis model was developed for the proposed retrofitted column that accounts for the effects of discontinuity of longitudinal reinforcement in the retrofit part. Comparison of pushover analysis and test results showed that the pushover model generally captured well the force-displacement behavior of the retrofitted columns.

1. Introduction

One of the common building types in Taiwan is the low-rise reinforced concrete (RC) row houses as shown in Fig. 1(a). The houses are usually three to five stories high and are built along streets. Due to the need for commercial use, parking garages, or living rooms, walls along the street direction in the first story of the house are usually eliminated (Fig. 1(b)). Moreover, rectangular columns with the weaker direction placed along the street direction are usually used to minimize the interference with the living space (Fig. 1(b)). As a result, during earthquake loading, these row houses are vulnerable to weak-story failure mechanism in the first story along the street direction. Figure 2 shows an example of weak-story failure of a row house in Taiwan during the 1999 Chi-Chi earthquake. It can be seen that the first story of the house was deformed significantly along the street direction while the stories above showed little damage.

Common seismic retrofit methods that can be used in row houses to improve the weak-story issue include RC jacketing [1-6], infill walls [7-8] and steel braces [9-10]. RC jacketing was considered in this research because infill walls and steel braces are often not welcomed by buildings owners as they can significantly interfere with the living spaces. Previous studies [1-6] have shown that RC jacketing is an effective seismic retrofit method for as-built RC columns. With an appropriate surface treatment of the as-built column, such as roughening [1, 5-6], steel connectors [3, 5-6], or dowels [3, 5], test results showed that columns retrofitted with RC jacketing were able to increase the flexural stiffness and strength to achieve similar behavior to counterpart monolithic columns. Some test results showed monolithic behavior can be nearly achieved even without any surface treatment of the as-built column [5-6]. However, some test results [3] showed that without any surface treatment to the as-built column, the damage was restricted to the RC jacket due to the loss of bond between the jacket and the as-built column, which resulted in a

sudden drop of strength after the maximum strength. In addition to enhancing the flexural behavior, RC jacketing can also enhance the shear strength of the column, thus resulting in better displacement ductility [2]. Despite the effectiveness of RC jacketing in seismic retrofit, conventional design of RC jacketing still requires additional living space.

An innovative retrofit method was proposed in this research to address the weak-story issue and to minimize the interference with the living space. In the proposed method, the rectangular columns at the corners of row houses in the first story (Fig. 3) are converted into L- or T-columns by adding flange sections on one or two sides of the column, respectively. The added flange sections occupy the space that would otherwise be occupied by non-structural walls, thus minimizing interference with the living space. The longitudinal reinforcement in the flange sections are not required to extend into the foundation or the beam, thus greatly increasing constructability. Three large-scale column specimens consisting of one L- and two T-columns retrofitted from rectangular columns were tested under cyclic loading. Test results were compared with monolithic L- and T-columns and original rectangular columns to investigate the effectiveness of the proposed retrofit method in increasing the lateral strength and seismic performance of as-built columns.

2. Experimental program

2.1. Specimen design

Three large-scale retrofitted column specimens were tested in this research. Two monolithic columns tested as part of an earlier investigation by the authors [11-12] were also included herein for comparison purpose. Table 1 lists the design parameters of the five columns including actual concrete and reinforcement strengths. The maximum aggregate size of the concrete was 20 mm.

The nomenclature for the column specimens is described as follows: "L" and "T" represent L- and T-columns, respectively; "M" and "R" represent monolithic and retrofitted columns, respectively; "C" and "W" represent a column or a wall design concept for the reinforcement in the retrofit part of the retrofitted column, respectively. Figure 4 shows the dimension and reinforcement design of the three retrofitted columns and two monolithic columns. The column specimens represent the lower half part of the first story column and hence were tested in a cantilever manner (single curvature) with lateral loading applied on the top of the specimens.

The three retrofitted columns were first constructed as rectangular columns with a section dimension of 350×600 mm and a design that is typical of columns currently used in row houses in Taiwan. After 28 days of curing, the rectangular columns were retrofitted to a L-column (column LRC) and two T-columns (columns TRC and TRW). The difference between columns TRC and TRW was the reinforcement design in the retrofit part of the column. The reinforcement design in the retrofit part of TRC followed the design concept of a column while that of TRW followed that of a wall. As a result, 14-D22 longitudinal bars and D10 transverse reinforcement spacing at 90 mm were used for TRC. In contrast, 10-D10 longitudinal bars and D10 transverse reinforcement spacing at 180 mm were used for TRW.

Because the retrofit part of the column in real application is located between a grade beam and a floor beam and post-installation of reinforcement into a beam is difficult due to dense longitudinal and transverse reinforcement, it was proposed in this research that longitudinal reinforcement in the retrofit part was not extended into the beams below and above the column. As a result, the longitudinal reinforcement in the retrofit parts of the three retrofitted columns were not continuous into the foundation of the specimen and hence was not effective to take flexural

tension. However, it was effective to take flexural compression and to provide confinement to core concrete together with transverse reinforcement.

The two monolithic columns, LM and TM, were designed to have the same nominal specimen geometry, amount of reinforcement, and material properties as retrofitted columns LRC and TRC, respectively. However, all the longitudinal reinforcement of LM and TM was extended into and properly anchored in the foundation and the loading block above the column. The two monolithic columns, LM and TM, were used to assess the performance of the two retrofitted columns, LRC and TRC, respectively.

2.2. *Construction of specimens*

The column specimens were constructed in two stages. In the first stage, three identical rectangular columns (350×600 mm) were constructed together with the foundation block and loading block. These rectangular columns represent the as-built columns of row houses to be retrofitted. After 28 days of curing, the second stage of construction was conducted to retrofit the columns by the proposed method to increase their seismic capacity along the weak direction. For the column representing those located at the four corners of the entire housing complex (Fig. 3), it was retrofitted into a L-column (column LRC). For the columns representing those located between different housing units (divided by partition walls) and in the front and back sides of the units, they were retrofitted into T-columns (column TRC and TRW) (Fig. 3).

In the second stage of construction, firstly, the cover concrete along the short side of the rectangular column was removed to reveal the reinforcement (Fig. 5(a)). The surface of the cover concrete along the long side of the column to be connected to the retrofit part was roughened to 6 mm amplitude [13] to increase the bond between the existing and new concrete. Next, additional

transverse reinforcement for the retrofit part was installed. For the L-column (LRC), one leg of the transverse reinforcement was post-installed into the column with an embedment length of 150 mm (Figs. 4(c) and 5(b)). The other parallel leg was welded to the transverse reinforcement of the original rectangular column using a single flare-v-groove weld (Figs. 4(c) and 5(c)). The size and length of the weld were greater than 0.6 times and 10 times the radius of the reinforcing bar, respectively [14]. For the T-columns (TRC and TRW), one leg of the transverse reinforcement was post-installed through the column (Figs. 4(d) and 4(e)). The hook at the end of the leg that went through the column was formed after going through the column. The other parallel leg was welded to the transverse reinforcement of the original rectangular column in the same way as column LRC (Figs. 4(d), 4(e) and 5(c)).

Thirdly, longitudinal reinforcement was installed. As stated previously, the longitudinal reinforcement was not extended into the foundation and only stayed within the retrofit part. Figures 5(d), 5(e), and 5(f) illustrate the reinforcement cages of columns LRC, TRC, and TRW, respectively. It can be seen that column TRC had larger longitudinal reinforcement and denser transverse reinforcement than column TRW as typically seen between reinforcement design for columns and that for walls. Finally, formwork was assembled and concrete was cast to form L- and T-columns. Cyclic tests were carried out after 28 days of curing.

2.3. Test setup

As stated previously, the columns were tested in a cantilever manner to simulate the behavior of the lower half part of the first story column. Figure 6 illustrates the test setup. Testing started first by applying an axial load by a 3000-kN actuator placed on the top of the column. An axial load of 622 kN and 1195 kN was applied to all the L-columns and to all the T-columns,

respectively. The resulting axial load ratio for each column was listed in Table 1. The axial load was applied uniformly over the entire cross section of the retrofitted column. Note that in real application, the axial load may not have a uniform distribution across the cross section. Most of the axial load is likely taken by the original part of the column. The effect of the axial load distribution was likely not significant because the level of the axial load was not high (Table 1), typical of the axial load conditions in low-rise buildings. The reaction to the axial load was provided by a load transfer beam that was placed on the top of the axial-load actuator and tied down to hinges fixed to the strong floor by two high-strength bars. Lateral cyclic loading was applied by a 2000-kN actuator that was attached to the reaction wall at one end and at the other end attached to loading block on the top of the column. The lateral load was applied to the centroid of the column cross section to minimize the effect of torsion, which was observed to be negligible during the testing. The foundation block of the specimen was fixed to the strong floor by four post-tensioned high-strength rods.

The lateral cyclic loading included drift levels of $\pm0.125\%$, $\pm0.25\%$, $\pm0.375\%$, $\pm0.5\%$, $\pm0.75\%$, $\pm1\%$, $\pm1.5\%$, $\pm2\%$, $\pm3\%$, $\pm4\%$, $\pm5\%$, $\pm6\%$, $\pm7\%$, $\pm8\%$, $\pm9\%$ and $\pm10\%$. Each drift level was repeated twice to examine the stiffness and strength degradation of the column. The drift was defined as the lateral displacement of the control point at the loading block on the top of the column divided by the distance from the control point to the top of the foundation (1700 mm). The displacement of the control point was measured by an optical sensor attached onto it. The sensor was a part of a three-dimensional motion capture system. During testing, the deformations of the column were monitored by 40-50 optical sensors attached on the side of the column and foundation parallel to the loading direction. Strain gauges were installed at various locations on the longitudinal and transverse reinforcement to capture the strains.

3. Test results and discussion

3.1. Crack patterns and damage conditions

Under cyclic loading, all the retrofitted columns exhibited ductile, flexural-dominant behavior. At the 0.375% drift, the interface of the retrofit part between the column base and the foundation started to crack. This interface crack soon became the dominant crack in the retrofit part. The crack opened when the retrofit part was loaded in tension. Under this condition, the retrofit part was not effective in providing strength because the longitudinal reinforcement in the retrofit part was not continuous into the foundation. When the loading direction was reversed and the retrofit part was in compression, the crack closed and the retrofit part became effective in providing strength by transferring compression to the foundation.

Figures 7(a)-(e) show the cracking and damage conditions of the two monolithic and three retrofitted columns at the peak load, 5% drift and end of the test. For all the columns, flexural cracks were initiated at drifts of 0.125%-0.25%. The first diagonal crack occurred at drifts of 0.375%-0.75%. The peak load was reached at drifts of 1%-2.95%. For the retrofitted columns, most of the flexural tensile deformation in the retrofit part was concentrated at the interface crack between the column base and foundation. This was because the flexural tensile resistance was much lower at the interface due to the fact that the longitudinal reinforcement was not extended across the interface and into the foundation. In contrast, for the monolithic columns, flexural tensile cracks spread more along the height of the column. At 5% drift, the monolithic columns had been severely damaged (Figs. 7(a) and 7(c)). The core concrete crushed and longitudinal reinforcement buckled or fractured. In contrast, less damage was observed in the retrofitted columns (Fig. 7(b),

7(d), and 7(e)) due to the discontinuity of the longitudinal reinforcement in the retrofit part at the column base. Most of the damage was limited to cover concrete. The retrofitted columns will require less effort to repair than the monolithic columns after earthquakes.

At 6% drift, the opening and closing of the interface crack of the retrofitted columns was more notable (Fig. 8). When the crack was closed and the retrofit part was compressed, crushing of core concrete and buckling of longitudinal reinforcement in the retrofit part were observed. When the loading direction was reversed, the crack opened up to 60 mm in width. After 6% drift, the bases of the two retrofitted parts of column TRW crushed significantly. Until the end of the testing, the column relied mainly on the original rectangular part of the column to resist lateral loading (Fig. 7(h)). In contrast, the extent of the damage in column TRC was less and hence the strength was better preserved (Fig. 7(g)). The denser transverse and larger longitudinal reinforcement used in the TRC than TRW provided better protection against crushing of core concrete and buckling of longitudinal reinforcement. No visible cracking or separation was observed along the interface between the retrofit and original parts of all the columns. The roughening applied to the surface of the original column appeared to be sufficient for a composite action between the retrofit and original parts of the columns.

3.2. *Hysteretic responses and force-drift envelope*

Figure 9 illustrates the hysteretic responses of the three retrofitted columns together with those of the counterpart monolithic columns. Important events observed during testing were marked on the hysteretic responses. The envelope of the hysteretic response of each column was idealized by a bilinear response according to FEMA 356 [15]. The first line segment of the bilinear response passed through the actual envelope at approximately 60% of the force of the idealized yield point,

which is the intersection point of the first and second line segments of the bilinear response. The second line segment ended at the ultimate point, which is defined as the point along the actual envelope response with a force dropped from the peak load by 20%. The idealized yield point was selected in order to balance the area below the actual envelope and the idealized bilinear response. The displacement ductility μ_{Δ} was then calculated by the drift at the ultimate point Δ_u divided by the drift at the idealized yield point Δ_y. The drifts at the idealized yield point, ultimate point and peak point, ductility calculated and peak loads are listed in Table 2.

$$\mu_{\Delta} = \frac{\Delta_u}{\Delta_y} \tag{1}$$

As shown in Fig 9(a), the lateral force resistance of column LRC in the negative direction was similar to that of column LM but that in the positive direction was 48% that of column LM. The reason was that in negative direction, the retrofit part was in compression and hence effective in providing strength. However, in the positive direction the retrofit part was lifted up and became ineffective in providing strength. Note that in real application, the behavior of the column will likely be in double curvature, which means in either loading directions (positive or negative), there will always be one end of the retrofit part in compression, more effective in providing strength, while the other end in tension, less effective in providing strength.

For column TRC (Fig. 9(b)), the force-displacement showed a symmetrical response because the two retrofit parts were symmetric. Column TRW (Fig. 9(c)) exhibited a similar behavior as TRC in term of initial stiffness and load capacity before the peak point. However, after 6% drift, the load capacity of TRW deteriorated much faster than that of TRC and resulted in an average of 28.7% lower ductility. The higher amount of transverse reinforcement and larger diameter of longitudinal reinforcement in the retrofit part of TRC than TRW delayed the speed of force

11

deterioration and resulted in better ductility. Compared with the monolithic counterpart, column TM, the average load capacities of TRC and TRW were 34% and 40% lower, respectively; however, the average displacement ductility were 75% and 25% higher, respectively (Table 2).

Figures 10(a) and 10(b) illustrate the force-drift envelopes of the retrofitted columns in comparison with those of the two monolithic columns. The pushover result of the original, unretrofitted column (Fig. 10(c)) was also shown in the figure. The pushover analysis was terminated due to crushing of the core, confined concrete of the column. Comparison of the test and analytical results showed that the proposed retrofit technique effectively increased the initial stiffness and load capacity of column LRC in the negative direction and columns TRC and TRW in both directions. The load capacities were approximately 120% higher in average (LRC in the negative direction and TRC and TRW in both directions) than that of the original, unretrofitted column. The load capacity of column LRC in the positive direction was almost identical to that of the original, unretrofitted column. This was because, in that direction, the retrofit part was not effective, as stated previously. The load capacity of column TRW approached that of the original, unretrofitted column at 8% drift while that of column TRC did not. This was consistent with the observed complete and partial crushing of concrete in the retrofit parts of columns TRW (Fig. 7(h)) and TRC (Fig. 7(g)), respectively. As stated previously, the difference was due to the lesser amount of reinforcement used in the retrofit part of TRW than TRC. Figure 11 shows the equivalent viscous damping ratios of all the columns. In general, the retrofitted columns showed lower energy dissipation than their monolithic counterparts. For example, at 4% drift, the average equivalent viscous damping ratio of the retrofitted columns was 74% that of their monolithic counterparts. This was due to the fact that the retrofitted column had less longitudinal reinforcement continuous into the foundation than their monolithic counterparts.

3.3.   Strain profile of longitudinal reinforcement

Figure 12(a) shows the strain development of the longitudinal reinforcement located near the column base in the original rectangular part for each of the three retrofitted columns. The reinforcement was able to develop high strains both in tension and compression. The tensile strains reached yield at drifts of 1-2%. Fig. 12(b) shows the strain profile of the longitudinal reinforcement located near the column base in the retrofit part for each of the columns. Because the reinforcement was not anchored into the foundation, it was only able to develop compressive strains. The compressive strains for columns TRC and TRW reached yield at drifts of 1% and 3%, respectively. The compressive strains for column LRC were significant at 3% drift but did not reach yield before malfunction of the strain gauge. It appeared that having longitudinal reinforcement in the retrofit part not effective in tension can be considered an advantage of the proposed retrofit method in terms of damage control. It minimized the tensile deformation of the reinforcement and hence delayed buckling of the reinforcement and damage to the surrounding concrete. Consequently, the retrofitted columns demonstrated much greater ductility than the monolithic counterparts.

3.4.   Curvature distribution and displacement composition

The deformations of the columns were calculated based on displacements recorded by optical sensors of a three-dimensional motion capture system as stated previously. The recording was terminated by removing all the optical sensors from the columns after 4% drift due to cracking and spalling of cover concrete. The deformations were separated into shear and flexural deformations for each column. It was found that the shear deformation of each column was small and accounted for less than 10% of the total lateral displacement. This was consistent with the observed flexural-dominated behavior of all the columns. The flexural deformations of each column are shown in

13

Fig. 13 in terms of curvatures. Note that the first curvature value is the average rotation from the column region 0 to 50 mm above the column base. Most of the rotation of this region was contributed by opening of the interface crack between the column and foundation.

From Fig. 13, it can be clearly seen that the curvature concentrated at the column base for column LRC in the positive direction and columns TRC and TRW in both directions. This was consistent with the observed significant opening of the interface crack between the column and foundation due to the discontinuity of longitudinal reinforcement as shown in Fig. 8. In contrast, the curvature distribution spread more towards the column top for the two monolithic columns as well as for column LRC in the negative direction. This was consistent with the observed crack patterns as shown in Fig. 7, in which cracks spread more along the column height for cases when the longitudinal tension reinforcement was anchored into the foundation such as the monolithic columns. Note that for column LRC in the negative loading direction, the tension side was on the original part of the column, in which the longitudinal tension reinforcement was anchored in the foundation same as the monolithic columns. Column TRW showed a sudden shifting of curvature towards the column top at 4% drift. This was due to the sudden spreading of concrete damage towards the column top at that drift. This was not seen for column TRC because it had better concrete confinement than TRW.

4. Pushover analysis model

A push-over analysis model was proposed to evaluate the behavior of the proposed retrofitted columns. The concepts used in the proposed pushover model can be easily integrated into existing pushover methods for performance evaluation of low-rise reinforced concrete structures (e.g. [16]) or used in the design of new houses to avoid the weak-story issue using the code method (e.g. [13])

or advanced method (e.g. [17]). To conduct the pushover analysis, material models for concrete and longitudinal reinforcement were derived first. The models were then used in the sectional moment-curvature analysis. Results of the analysis were converted to obtain the relationship between lateral force and flexural displacement of the column. The flexural displacement was then added with displacements contributed by bar slip and shear to obtain the total lateral displacement. The details of the material models, sectional model and calculation methods of displacements contributed by flexure, bar slip, and shear are described in sequence as follows.

Among the various models for concrete compressive behavior [18], Mander confined and unconfined models [19] were used to model the core and cover concrete, respectively (Fig. 14(a)). In deriving the Mander confined concrete model, the confinement effectiveness coefficient k_e was a key parameter but was not discussed for L- and T- columns in the original publication. Based on the definition of the k_e, i.e., the effectively confined core to the nominal core area bounded by the centerline of the peripheral hoops, Eq. (4) was proposed to calculate the k_e for L- and T-columns. The effectively confined cores of L- and T-column are illustrated in Fig. 15.

$$k_e = \frac{\left(A_c - \sum w^2{}_i/6\right)}{\left(A_c - A_s\right)} \times \frac{A_{cm}}{A_c} \tag{4}$$

where A_c = the area of core section enclosed by the center lines of perimeter hoops; A_{cm} = the area of core section at midway between levels of transverse reinforcement; A_s = the total cross-sectional area of longitudinal reinforcement; and w_i = the i-th clear transverse spacing between two laterally supported longitudinal reinforcement bars. Note that the original part did not have the same concrete strength as the retrofit part as shown in Table 1. The tensile strength of concrete was ignored. The tensile behavior of longitudinal reinforcement in the original part of the column was simulated using the strain-hardening steel model as shown in Fig. 14(b). The model consists

15

of a linear relationship between the stress and strain before yielding and after yielding a yield plateau followed by a strain-hardening branch. The longitudinal reinforcement in the retrofit part was assumed to take no tension because it was not continuous into the foundation and the test results have showed insignificant tensile responses in such reinforcement (Fig. 12(b)). The compressive behavior of longitudinal reinforcement in both the original and retrofit parts consists of a linear elastic branch same as the tensile behavior. However, the post-yielding branch is deteriorated from the tensile post-yielding behavior to reflect the effect of buckling [20, 21] as shown in Fig. 14(b). From Fig. 14(b), it can be seen that the compressive behavior of longitudinal reinforcement in the retrofit part of column TRW deteriorates much faster than that of column TRC because of a smaller diameter of longitudinal reinforcement and a lesser amount of transverse reinforcement. This together with less concrete confinement lead to a faster drop in the post-peak behavior of column TRW than column TRC as observed from tests. The ultimate strain of the longitudinal reinforcement was set equal to $0.7\varepsilon_{su}$ [22], where $\varepsilon_{su} = 0.12$.

Sectional moment-curvature analysis was conducted based on the fiber section model as shown in Fig. 16. The material models defined above were input into the concrete and steel fibers of the fiber section model. Actual material strengths were used (Table 1). The moment-curvature analysis was conducted until either the core concrete or the reinforcement in the original part of the column reached their ultimate strains.

The total displacement of the column consists of three components contributed by flexure, bar slip, and shear.

$$\Delta_{total} = \Delta_{flexure} + \Delta_{slip} + \Delta_{shear} \tag{5}$$

where $\Delta_{flexural}$, Δ_{slip}, and Δ_{shear} = displacements contributed by flexure, bar slip, and shear, respectively. The flexural displacement $\Delta_{flexural}$ was calculated by

$$\Delta_{flexural} = \Delta_y + \Delta_p \tag{6}$$

$$\Delta_y = \phi_y L^2 / 3 \tag{7}$$

$$\Delta_p = \left(\phi_u - \phi_y\right) L_p \left(L - 0.5 L_p\right) \tag{8}$$

where Δ_y and Δ_p = displacements at the yield point and ultimate point, respectively; ϕ_y and ϕ_u = curvatures at the yield point and ultimate point, respectively; L = the column height; and L_p = the plastic hinge length. A plastic hinge length L_p of $0.5D$ was used [23], where D = sectional depth from the extreme compression fiber of the whole section to extreme tension fiber of the original section. Figure 17 illustrates the definition of D. The retrofit part is included in D only when it is in compression.

The bar-slip displacement Δ_{slip} is the lateral displacement caused by the slip of longitudinal reinforcement out of the foundation (Fig. 17). It was calculated based on the bar-slip model proposed by Sezen et al. [24] defined as follows.

$$\Delta_{slip} = \theta_{slip} L \tag{9}$$

$$\theta_{slip} = \delta_{slip} / \left(d_{slip} - c\right) \tag{10}$$

$$\delta_{slip} = \frac{\varepsilon_y}{2} L_d + \frac{\left(\varepsilon_y + \varepsilon_s\right)}{2} L_d' \tag{11}$$

$$L_d = f_y d_b / 4 u_b \tag{12}$$

$$L_d' = \left(f_s - f_y\right) d_b / 4 u_b' \tag{13}$$

where θ_{slip} = the rotation due to the bar slip (Fig. 17); δ_{slip} = the slip of the bar; d_{slip} = the distance from the longitudinal bar from which the bar slip δ_{slip} is calculated to the extreme compression

fiber of the section; c = the neutral axis depth; ε_y and f_y = the yield strain and stress of the longitudinal bar, respectively; ε_s and f_s = the strain and stress of the longitudinal bar, respectively; L_d and L_d' = development lengths for the elastic portion and inelastic portion of the longitudinal bar, respectively; and u_b and u_b' = uniform bond strengths for the elastic portion ($\sqrt{f_c'(\mathrm{MPa})}$) and inelastic portion ($0.5\sqrt{f_c'(\mathrm{MPa})}$) of the longitudinal bar, respectively . In this research, the extreme layer of longitudinal tension reinforcement was used to calculate the bar-slip displacement. Note that only the original part of the column had longitudinal tension reinforcement. The longitudinal reinforcement in the retrofit part was assumed to resist only compression.

The shear deformation Δ_{shear} before diagonal cracking was calculated based on the shear stiffness as defined by Eq. (13) [25].

$$K_v' = \frac{0.4E_c b_w d}{f} \tag{13}$$

where K_v'=the shear stiffness before diagonal cracking of one unit length; E_c=the modulus of elasticity of concrete; b_w=the width of the column web; and f=the form factor and is equal to 1.2 for rectangular sections and 1.0 for I- and T-sections. After diagonal cracking, the shear deformation was calculated based on the truss action as defined by Eq. (14) [25]. Equation (14) is reduced to Eq. (15) when the shear crack angle is 45 degrees and the stirrups are perpendicular to the axis of the column, which is the case of this investigation.

$$K_v = \frac{\rho_v \sin^4 \alpha \sin^4 \beta (\cot \alpha + \cot \beta)^2}{\sin^4 \alpha + n\rho_v \sin^4 \beta} E_s b_w d \tag{14}$$

$$K_{v,45} = \frac{\rho_v}{1+4n\rho_v} E_s b_w d \tag{15}$$

where K_v and $K_{v,45}$ = the shear stiffness after diagonal cracking and that with the shear crack angle equal to 45 degrees and the stirrups perpendicular to the axis of the column; ρ_v = the transverse reinforcement ratio inside the web area $b_w d$; α and β = the inclined angles of the compression struts and stirrups, respectively; n = the modular ratio of steel to concrete E_s/E_c; and E_s =the modulus of elasticity of concrete.

Figure 18 shows the comparison between the analytical pushover and measured hysteretic behavior for each retrofitted column. Good agreement can be observed for the initial stiffness and the peak load. The post-peak deterioration of the pushover curve was initiated by the crushing of concrete in the retrofit part, which matched the test observation. All the push-over analyses terminated when the core concrete of the original part reached its ultimate compressive strain. In the positive loading direction of column LRC, the test showed an earlier drop of the force than the prediction. As observed from the test result (Fig. 7(f)), this earlier drop was due to crushing of core concrete with the anchorage failure of transverse reinforcement. Such a failure mode cannot be captured by the proposed model. The predicted failure mode was also crushing of core concrete but initiated by fracture of transverse reinforcement. Another reason for earlier drop than predicted was due to the fact that for the same drift, more damage was caused by cyclic loading than pushover loading. The pushover analysis showed that column TRC could have been tested to higher drifts until the core concrete in the original part was crushed. The test was terminated prematurely due to safety concerns. Earlier termination of The difference between pushover

19

5. Conclusion

An innovative seismic retrofit method was proposed in this research to turn rectangular columns in the first story into L- and T-columns to address the weak-story issue. An experimental study was conducted to investigate the seismic behavior of columns retrofitted with the proposed retrofit method. Main conclusions are summarized as follows.

(1) Under cyclic loading, all the retrofitted L- and T-columns showed ductile, flexural-dominated behavior. With the procedure used in this research for improving the bond of the interface between the original and retrofit parts of the columns, no visible cracking or separation was observed along the interface during testing. The proposed retrofitted method can increase the load capacities by approximately 120% in average for the columns examined in this research.

(2) The strain readings showed that the longitudinal reinforcement in the retrofit parts of the columns was effective only in compression due to discontinuity of the longitudinal reinforcement at the column base. Therefore, the retrofitted columns showed lower lateral strengths than the counterpart monolithic columns. However, the retrofitted columns showed less damage in concrete and reinforcement and hence exhibited higher ductility ratios than the counterpart monolithic columns. The retrofitted column with a reinforcement design typical of a column showed a similar lateral strength to but a significantly higher ductility ratio than that with a reinforcement design typical of a wall.

(3) A pushover analysis model was developed for the proposed retrofitted columns. The model is based on available constitutive models in the literature with modifications to account for the effects of discontinuity of longitudinal reinforcement in the retrofit part at the column base. Comparison of the pushover analysis results with the test results showed that the initial

stiffness, lateral strength, and the general trend of the post-peak behavior were well captured by the proposed pushover model.

6. Acknowledgement

7. References

[1] Rodriguez, M. and R. Park, Seismic load tests on reinforced concrete columns strengthened by jacketing. Structural Journal, 1994. 91(2): p. 150-159.

[2] Fukuyama, K., Y. Higashibata, and Y. Miyauchi, Studies on repair and strengthening methods of damaged reinforced concrete columns. Cement and Concrete Composites, 2000. 22(1): p. 81-88.

[3] Vandoros, K.G. and S.E. Dritsos, Concrete jacket construction detail effectiveness when strengthening RC columns. Construction and Building Materials, 2008. 22(3): p. 264-276.

[4] Bousias, S.N., A.-L. Spathis, and M.N. Fardis, Concrete or FRP jacketing of columns with lap splices for seismic rehabilitation. Journal of Advanced Concrete Technology, 2006. 4(3): p. 431-444.

[5] Bousias, S.N., et al., Strength, stiffness, and cyclic deformation capacity of concrete jacketed members. ACI Structural Journal, 2007. 104(5): p. 521-531.

[6] Júlio, E.N. and F.A. Branco, Reinforced concrete jacketing-Interface influence on cyclic loading response. ACI Structural Journal, 2008, 105(4): p. 471-477.

[7] Sonuvar MO, Ozcebe G, Ersoy U. Rehabilitation of reinforced concrete frames with reinforced concrete infills. Structural Journal, 2004, 101(4):494-500.

[8] Altin S, Anil Ö, Kara ME. Strengthening of RC nonductile frames with RC infills: An experimental study. Cement and Concrete Composites, 2008, 30(7):612-621.

[9] Youssef MA, Ghaffarzadeh H, Nehdi M. Seismic performance of RC frames with concentric internal steel bracing. Engineering Structures, 2007, 29(7):1561-1568.

[10] Mahrenholtz C, Lin PC, Wu AC, Tsai KC, Hwang SJ, Lin RY, Bhayusukma MY, Retrofit of reinforced concrete frames with buckling-restrained braces. Earthquake Engineering & Structural Dynamics, 2015, 44(1):59-78.

[11] Ou, Y.C., Truong, A.N., Cyclic flexural and shear behavior of reinforced concrete L- and T-columns, ACI Structural Journal, 2018.

[12] Truong, An-Nhien, Cyclic Behavior of L- and T-shaped Reinforced Concrete Columns. Master dissertation, Taipei, Taiwan: National University of Science and Technology, 2016.

[13] ACI Committee 318, Building Code Requirements for Structural Concrete (ACI 318-14) and Commentary. American Concrete Institute, Farmington Hills, MI, 2014.

[14] AWS, D1.4/D1. 4M, Structural Welding - Reinforcing Steel. American Welding Society, Miami, FL, 2005.

[15] FEMA 356. Prestandard and commentary for seismic rehabilitation of buildings. Washington, DC, USA: Federal Emergency Management Agency, 2000.

[16] Hsiao, F.P., Oktavianus, Y., Ou, Y.C., Luu, C.H., and Hwang, S.J., A pushover seismic analysis and retrofitting method applied to low-rise RC school buildings. Advances in Structural Engineering, 2015, 18(3), 311-324.

[17] Montuori, R., Muscati, R., Smart and simple design of seismic resistant reinforced concrete frame. Composites Part B: Engineering, 2017, 115, pp. 360-368.

[18] Cavaleri, L., Trapani, F.D., Ferrotto, M.F., Davì, L., Stress-strain models for normal and high strength confined concrete: Test and comparison of literature models reliability in reproducing experimental results. Ingegneria Sismica, 2017, 34 (3-4), pp. 114-137.

[19] Mander, John B., Michael JN Priestley, and R. Park, Theoretical stress-strain model for confined concrete. Journal of Structural Engineering, 1988, 114, No. 8: 1804-1826.

[20] Dhakal, Rajesh Prasad, and Koichi Maekawa, Reinforcement Stability and Fracture of Cover Concrete in Reinforced Concrete Members, 2002, 128, No. 9: 1253-1262.

[21] Dhakal, Rajesh Prasad, and Koichi Maekawa. Path-dependent cyclic stress–strain relationship of reinforcing bar including buckling. Engineering Structures, 2002, 24, No. 11: 1383-1396.

[22] Ou, Y.C., and Nguyen, D.N, Modified axial-shear-flexure interaction approaches for uncorroded and corroded reinforced concrete beams. Engineering Structures, 2016, 128, 44-54.

[23] Ou, Y.C., Chiewanichakorn, M., Aref, A.J., and Lee, G.C, Seismic performance of segmental precast unbonded posttensioned concrete bridge columns. Journal of Structural Engineering, ASCE, 2007, 133(11), 1636-1647.

[24] Sezen, Halil, and Eric J. Setzler, Reinforcement slip in reinforced concrete columns. ACI Structural Journal, 2008, 105, No. 3: 280.

[25] Park, Robert, and Thomas Paulay, Reinforced concrete structures. John Wiley & Sons, 1975.

LIST OF TABLES

Table 1. Column design parameters

Column	f'_c, MPa	f'_{ca}, MPa	f'_{car}, MPa	Axial load ratio, $P/f'_{cav}A_g$	Shear span, a/d	Transverse reinforcement				Longitudinal reinforcement			
						f_{yh}, MPa	f_{yha}, MPa	Size@spacing, mm	ρ_{sh}, %	f_y, MPa	f_{ya}, MPa	Quantity-size	ρ_g, %
LM [11-12]	21	23.6	N.A.	0.088	3.62	280	379	D10 @ 90	0.69	420	487	21-D22[c]	2.68
TM [11-12]		32.2	N.A.	0.097	2.47			D10 @ 90	0.67			28-D22[c]	2.76
LRC		23.6	28.5	0.084	3.62			D10 @ 90[a] +D10 @ 90[b]	0.69			14-D22[c] +7-D22[d]	2.68
TRC		32.2	28.5	0.102	2.47			D10 @ 90[a] +D10 @ 90[b]	0.67			14-D22[c] +14-D22[d]	2.76
TRW		31.8	28.5	0.102				D10 @ 90[a] +D10 @ 180[b]	0.45	280	379	14-D22[c] +10-D10[d]	1.58

Note: f'_c = the nominal compressive strength of concrete; f'_{ca} and f'_{car} = the actual compressive strength of the original part and retrofit part, respectively; P = the applied axial force; f'_{cav} = the average compressive strength of concrete; A_g = the gross area of concrete cross section; a = shear span, equal to the distance from the lateral load point to the top surface of the foundation; d = effective depth of the section measured from extreme compression fiber to the resultant tensile force of longitudinal reinforcement; f_{yh} and f_{yha} = the nominal and actual yield strength transverse reinforcement, respectively; f_y and f_{ya} = the specified and actual yield strength of longitudinal reinforcement, respectively; ρ_{sh} = the volumetric ratio; ρ_g = the ratio of longitudinal reinforcement area to the gross area.
[a]: transverse reinforcement in the original part; [b]: transverse reinforcement in the retrofit part; [c]: longitudinal reinforcement in the original part; [d]: longitudinal reinforcement in the retrofit part.

Table 2. Lateral force - displacement capacities

Column	Idealized yield drift %		Peak load, kN		Peak load drift, %		Ultimate drift, %		Displacement ductility	
	(1)	(2)	(3)	(4)	(5)	(6)	(7)	(8)	(9)	(10)
	−	+	−	+	−	+	−	+	−	+
LM [11-12]	−0.90	+0.80	−459	+465	−1.89	1.92	−5.00	+5.25	5.56	6.56
TM [11-12]	−0.63	+0.65	−828	+762	−1.36	1.78	−4.30	+4.55	6.83	7.00
LRC	−0.80	+0.43	−433	+222	−2.95	1.85	−5.18	+5.84	6.48	13.58
TRC	−0.40	+0.40	−517	+540	−2.81	1.31	−5.18	+4.50	12.95	11.25
TRW	−0.40	+0.40	−476	+490	−1.01	1.01	−3.90	+3.00	9.75	7.50

Note:"−" and "+" indicates the loading in negative and positive direction, respectively.

LIST OF FIGURES

Fig. 1. (a) Typical row houses in Taiwan; and (b) plan view of the first story of typical row houses

Fig. 2. Failure of the first story of row houses along the street direction during the 1999 Chi-Chi earthquake
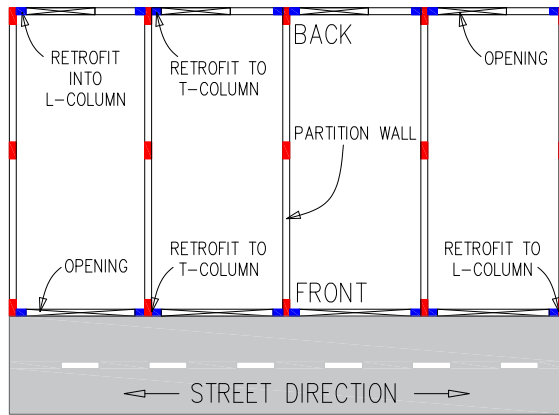
Fig. 3. Plan view of the first story with proposed retrofitted columns
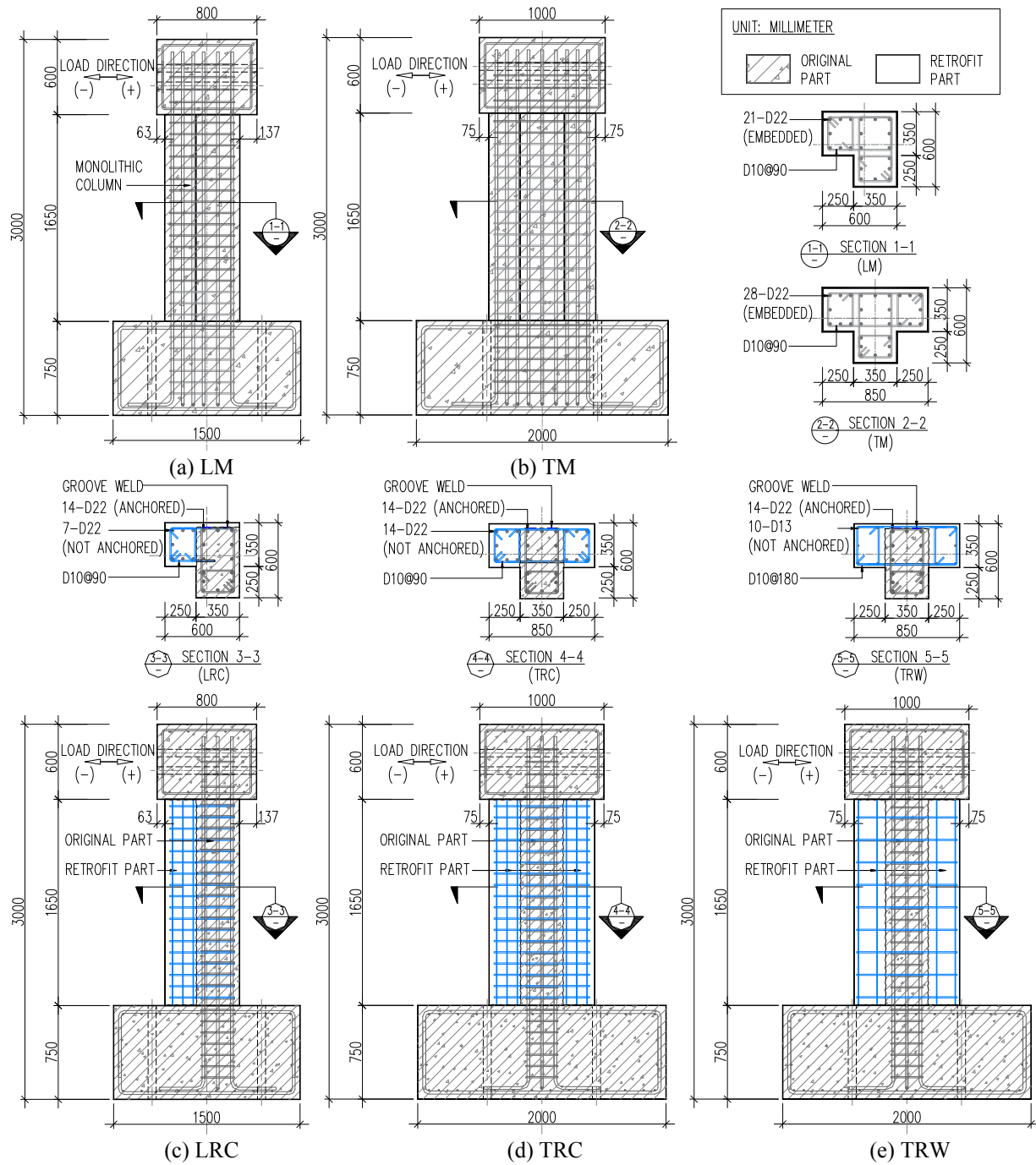
Fig. 4. Reinforcement and cross-sectional details for column: (a) LM; (b) TM; (c) LRC; (d) TRC; and (e) TRW

<center>(a)   (b)   (c)</center>
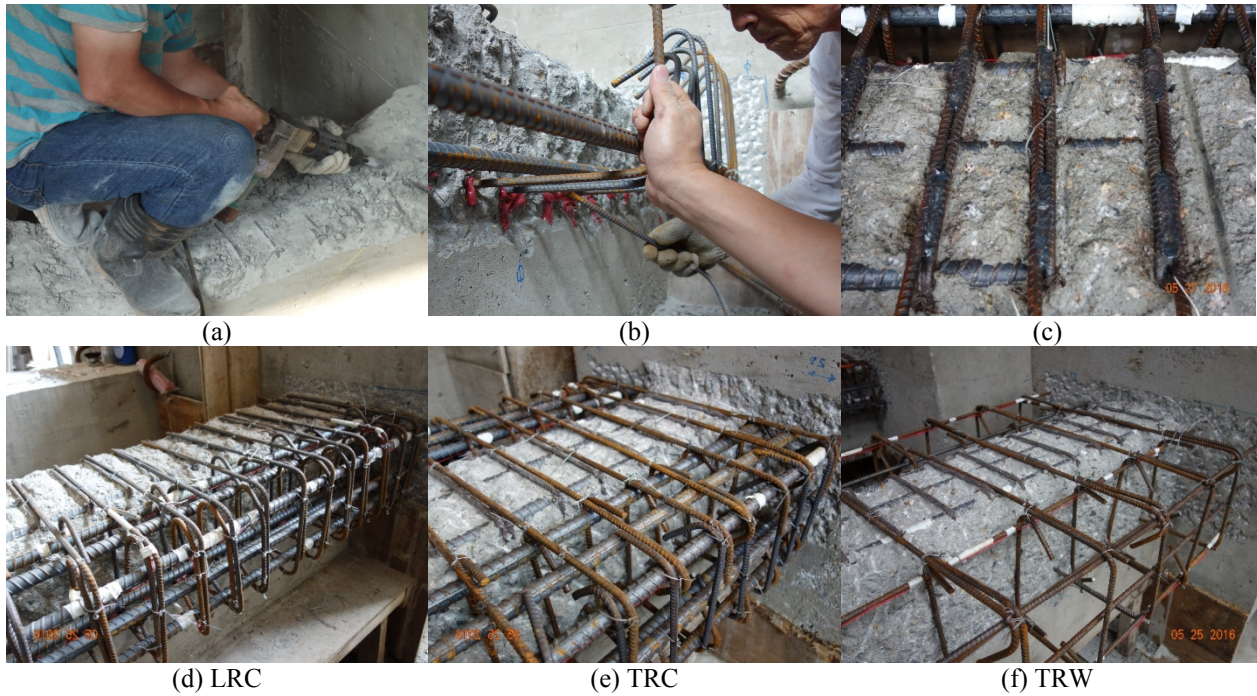
<center>(d) LRC   (e) TRC   (f) TRW</center>

Fig. 5. (a) Removing the cover concrete and roughening the surface; (b) post-installation of transverse reinforcement; (c) welding of transverse reinforcement; reinforcement cage for column: (d) LRC; (e) TRC, and (f) TRW

<center>33</center>
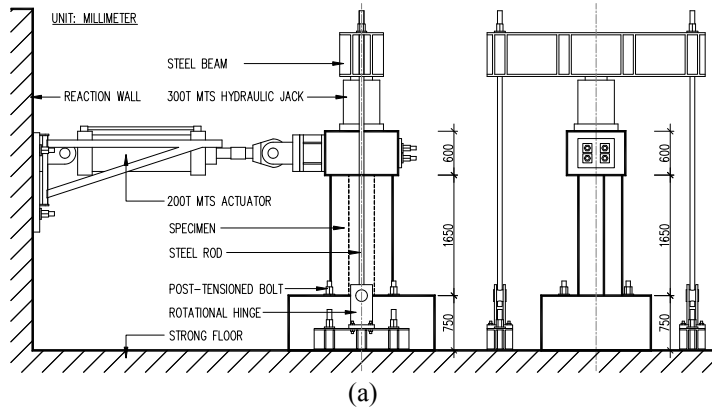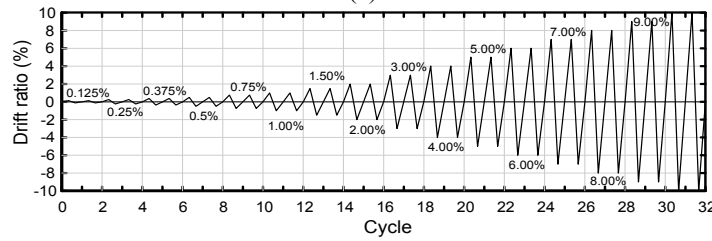
Fig. 6. (a) Test setup; (b) loading protocol; and (c) photo of test setup
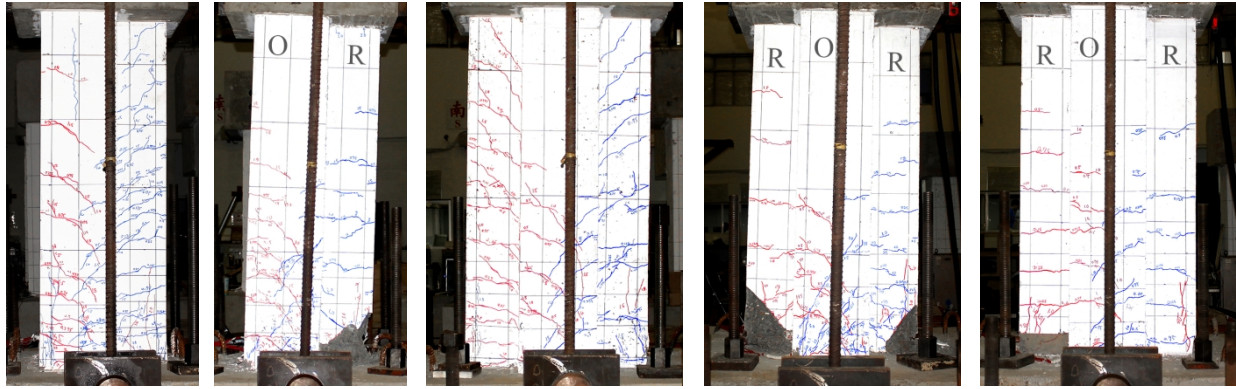
Peak load
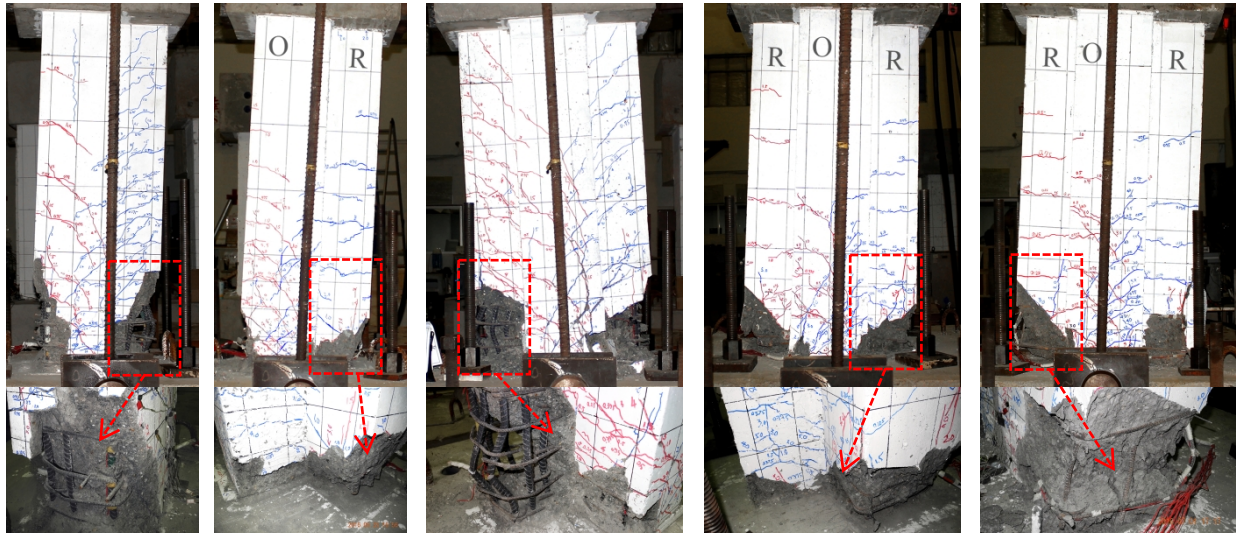
5% drift
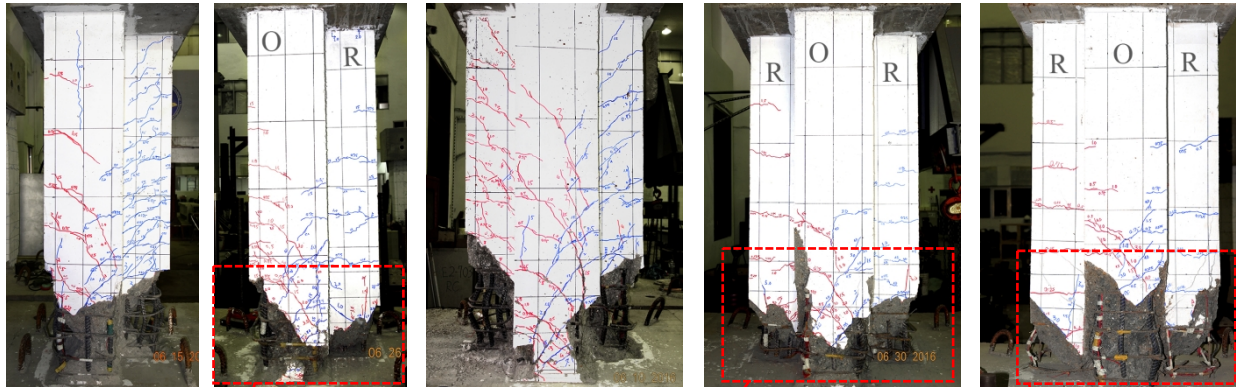
End of test

(a) LM   (b) LRC   (c) TM   (d) TRC   (e) TRW
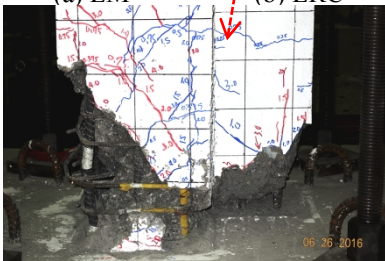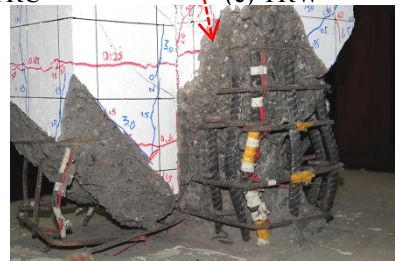
(f)   (g)   (h)

Fig. 7. Damage conditions at peak load, 5% drift, and end of test for column: (a)LM; (b) LRC; (c) TM, (d) TRC; and (e) TRW; "O" and "R" refer to the original part and the retrofit part, respectively

Opening of the interface between the column and foundation

Closing of the interface between the column and foundation

(a) LRC   (b) TRC   (c) TRW

Fig. 8. Opening and closing of the interface between the column and foundation for column (at

6% drift): (a) LRC; (b) TRC; and TRW
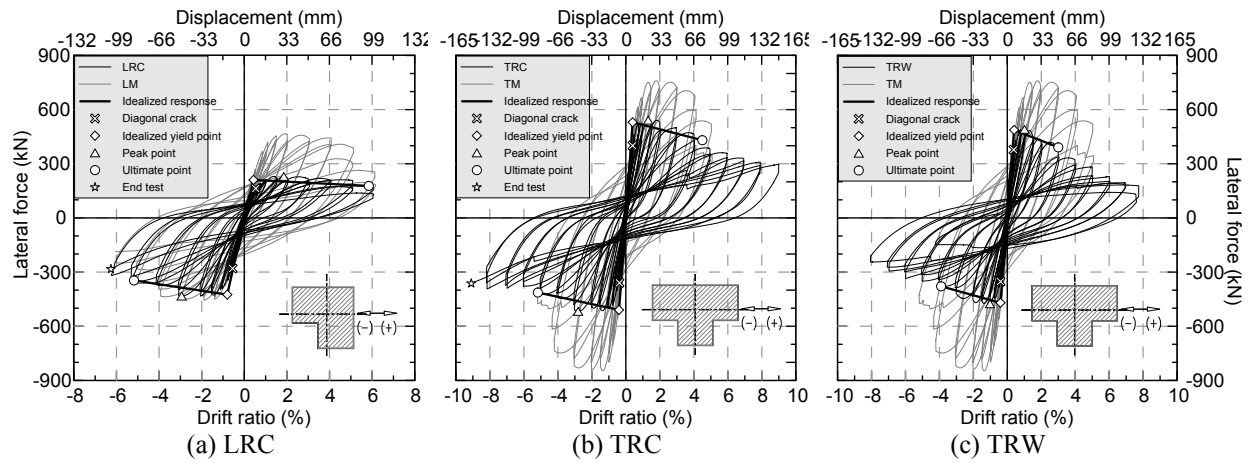
Fig. 9. Hysteretic behavior of column: (a) LRC; (b) TRC; and (c) TRW
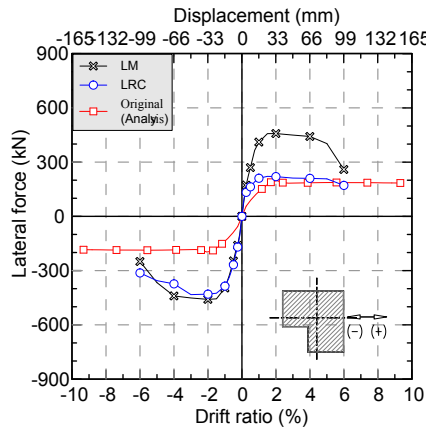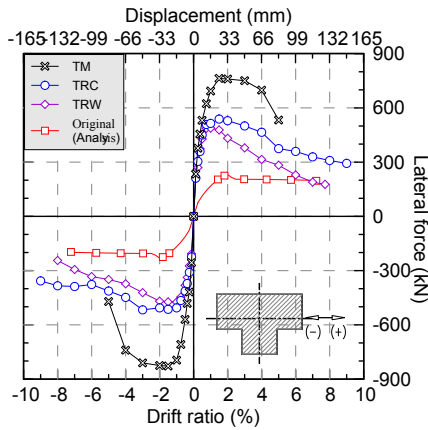
(a) L-columns   (b) T-columns   (c) Original column
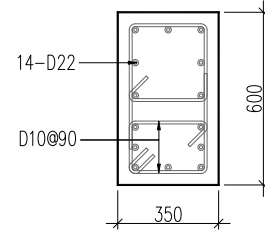
Fig. 10. Force-drift envelopes of: (a) L-columns; and (b) T-columns; and (c) original column
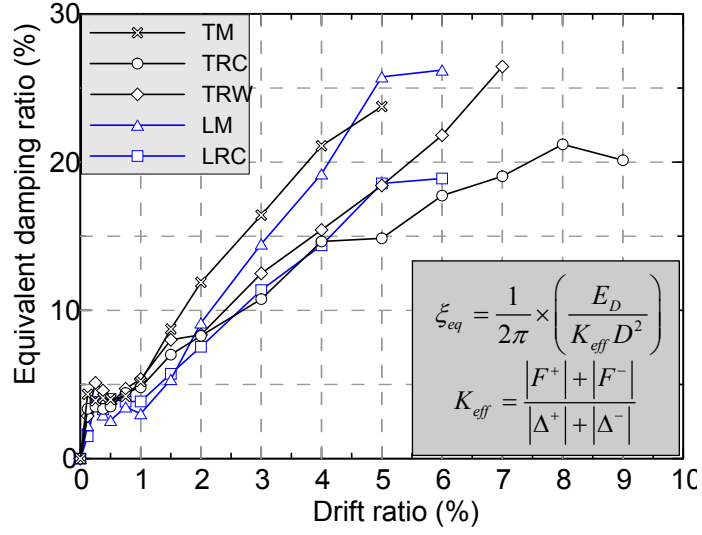
Note: ξ_{eq} = the equivalent viscous damping ratio; E_D = the energy dissipation of a hysteretic loop; K_{eff} = the effective stiffness; D = the maximum displacement of a hysteretic loop; Δ^-, Δ^+ = the maximum positive and negative displacement of a hysteretic loop, respectively; and F^-, F^+ = the force corresponding to Δ^-, Δ^+, respectively.

Fig. 11. Equivalent damping ratios
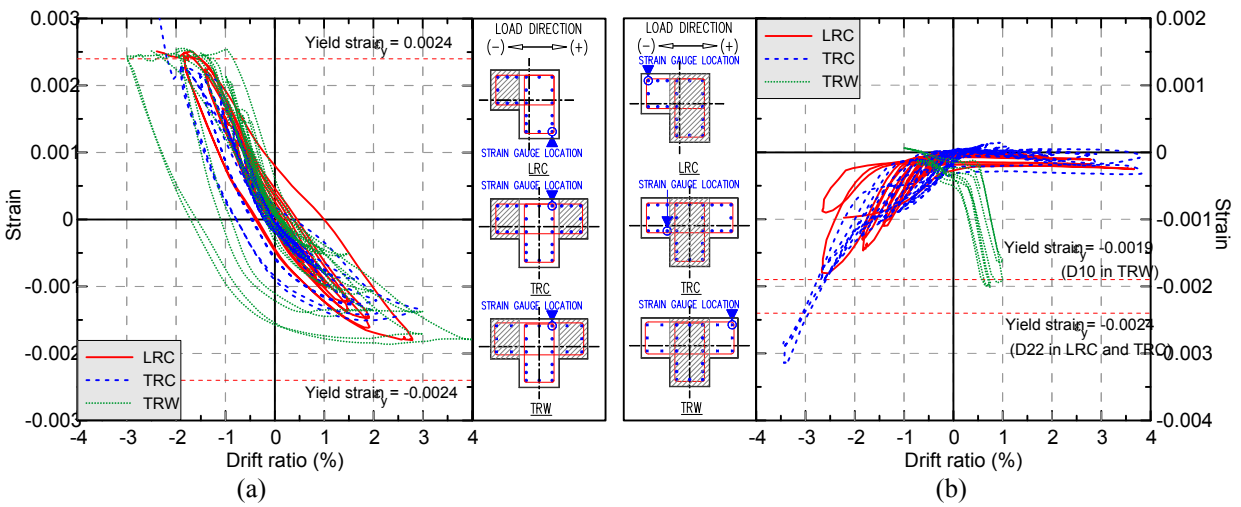
Fig. 12. Selective strains in longitudinal reinforcement at the base of the column: (a) in the original part; and (b) in the retrofit part
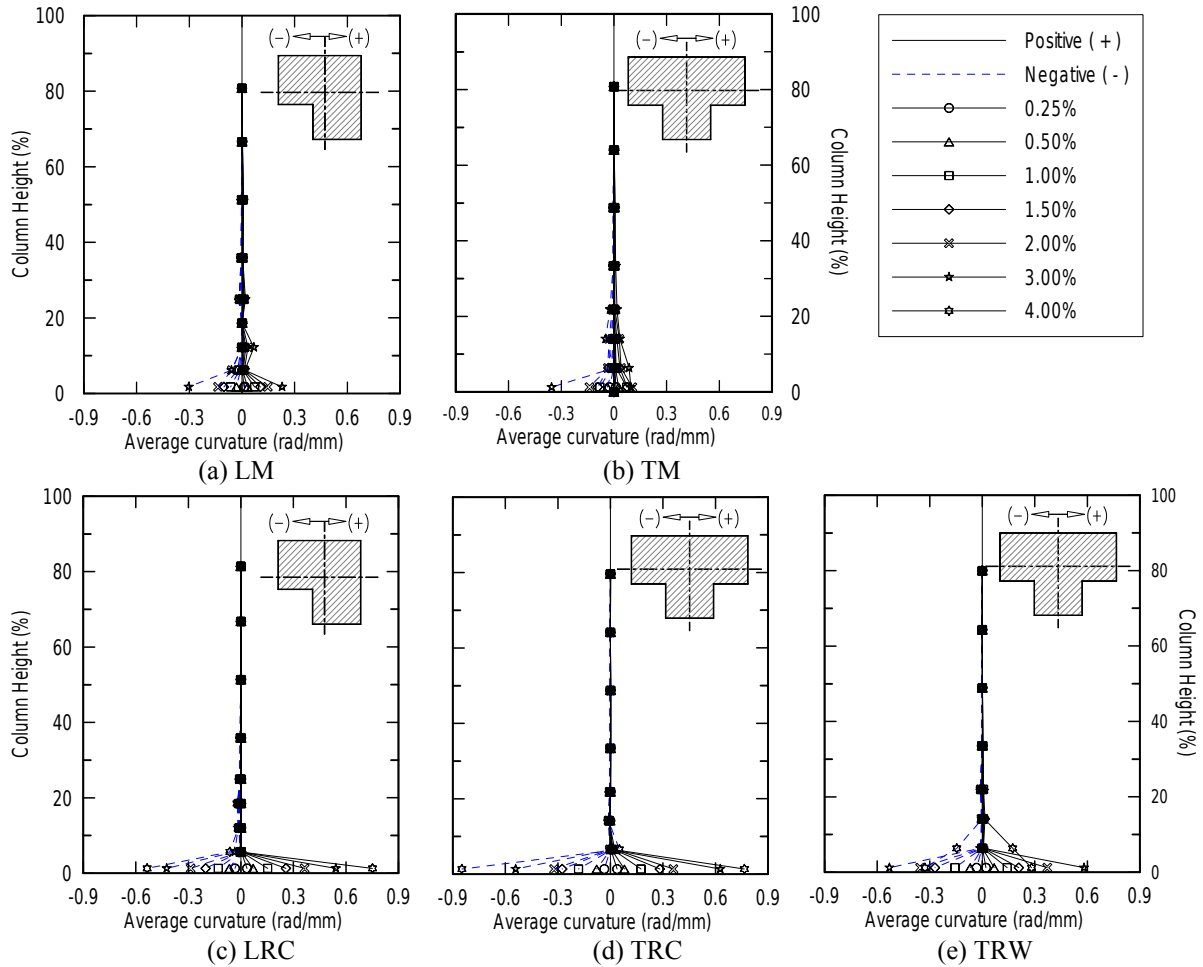
Fig. 13. Curvature distribution for column: (a) LM; (b) TM; (c) LRC; (d) TRC; and (e) TWC
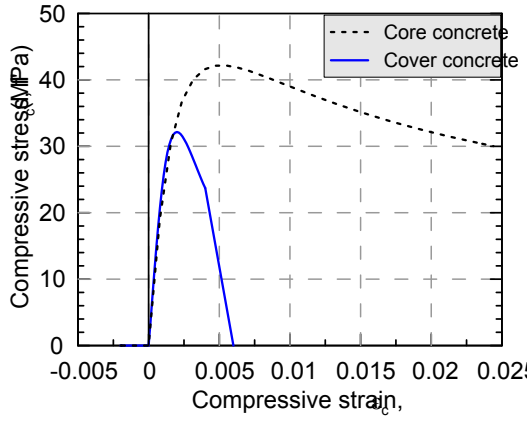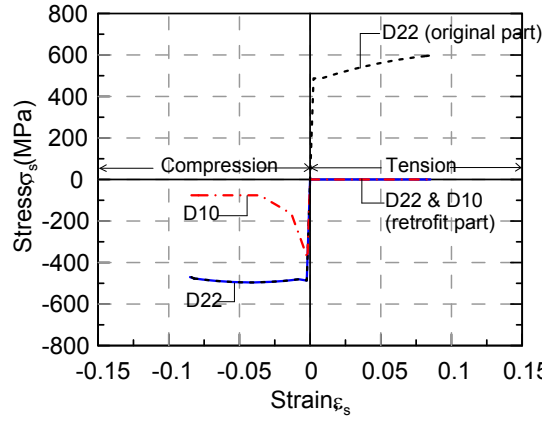
(a) Concrete   (b) Steel reinforcement

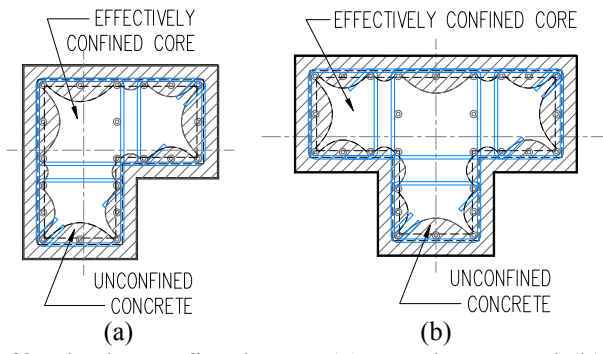**Fig. 14.** Material models: (a) concrete; and (b) steel reinforcement

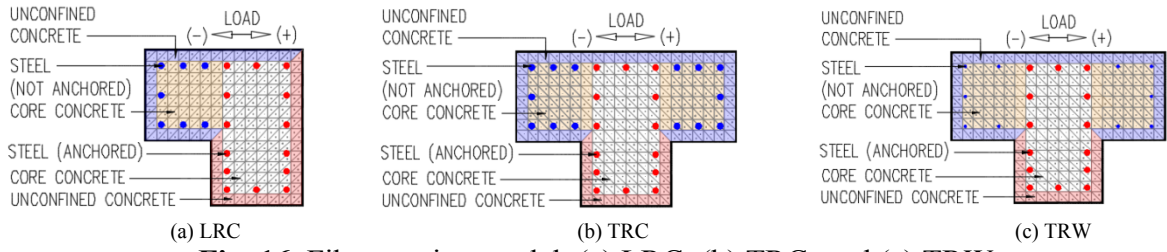**Fig. 15.** Effectively confined area: (a) L-column; and (b) T-column

(a) LRC   (b) TRC   (c) TRW

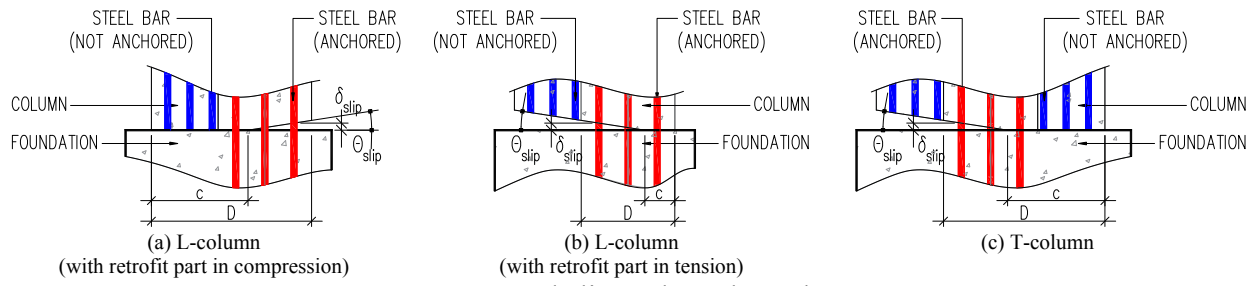**Fig. 16.** Fiber section model: (a) LRC; (b) TRC; and (c) TRW

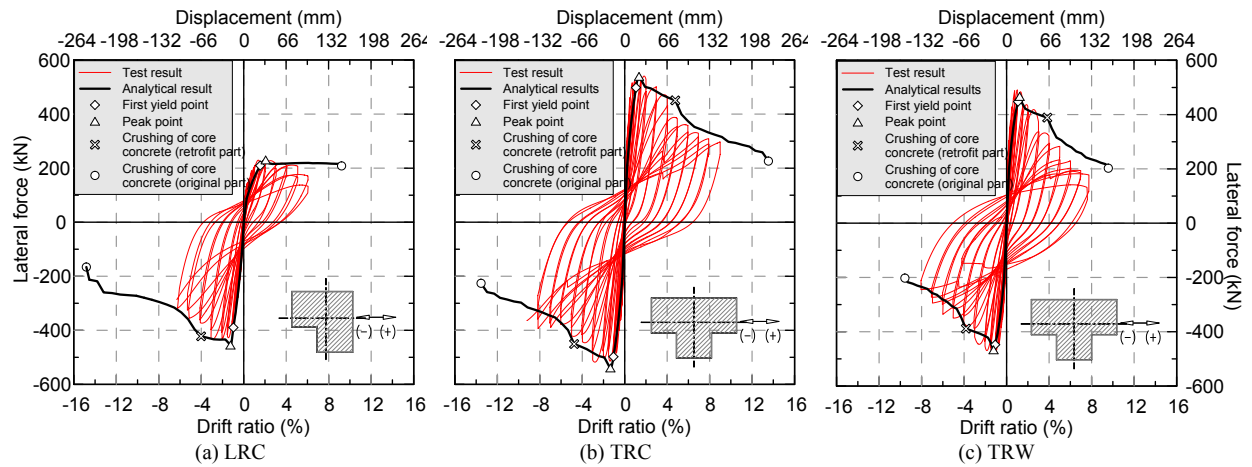**Fig. 17.** Bond slip at the column base

Fig. 18. Comparisons of analytical study and experimental hysteretic responses